Dalton Transactions

ROYAL SOCIETY OF CHEMISTRY

PAPER

View Article Online
View Journal

Cite this: DOI: 10.1039/d1dt03465k

Growth modulation of atomic layer deposition of HfO_2 by combinations of H_2O and O_3 reactants†

Byeong Guk Ko,‡[a] Chi Thang Nguyen,‡[a] Bonwook Gu,[a] Mohammad Rizwan Khan,[a] Kunwoo Park,[b] Hongjun Oh,[c] Jungwon Park,[b] Bonggeun Shong[c] and Han-Bo-Ram Lee*[a]

Received 14th October 2021,
Accepted 20th November 2021

DOI: 10.1039/d1dt03465k

rsc.li/dalton

Atomic layer deposition (ALD) is a thin film deposition technique based on self-saturated reactions between a precursor and reactant vacuum conditions. A typical ALD reaction consists of the first half-reaction of the precursor and the second half-reaction of the counter reactant, in which the terminal groups on the surface change after each half-reaction. In this study, the effects of counter reactants on the surface termination and growth characteristics of ALD HfO_2 thin films formed on Si substrates using tetrakis(dimethylamino)-hafnium (TDMAH) as a precursor were investigated. Two counter reactants, H_2O and O_3, were individually employed, as well as in combination with consecutive exposure by H_2O–O_3 and O_3–H_2O. The film growth behaviors and properties differed when the sequence of exposure of the substrate to the reactants was varied. Based on X-ray photoelectron spectroscopy (XPS) and density functional theory (DFT) simulation, the changes are attributed to the effects of the surface terminations formed from different counter reactant combinations. The knowledge from this work could provide insight for precisely tuning the growth and properties of ALD films.

1. Introduction

The characteristic features of atomic layer deposition (ALD), such as large-area uniformity, ability to cover meter-scale substrates, excellent step coverage in 3D nanostructures, and precise thickness control at the atomic scale[1–4] have made this process a prominent technique for depositing thin films for fabricating nanoscale devices. The growth of thin films by ALD is performed in a layer-by-layer manner through a self-saturated surface reaction mechanism by alternate exposure of the substrate to the precursors.[4–7] Because the surface reactions under saturation conditions limit the growth to one monolayer at each cycle, atomic-scale thickness control is achieved during ALD film growth. Therefore, film growth using ALD is strongly affected by the chemical species on the surface. For example, the growth rates of the ALD films differ even on the same substrate if surface terminations are different, such as H, OH, and O terminations at the initial growth.[8–10]

In addition to the surface species and materials, film growth depends on the surface chemical terminations formed by the precursors, the reactants used for ALD, and the original surface species.[8–13] Various oxygen source, such as H_2O, H_2O_2, O_2, O_3, and O_2 plasma, have been used as reactants for ALD,[14–17] where these reactants generate different surface terminations during the reactant half-reaction,[18,19] resulting in different growth rates.[20,21] Therefore, the growth rate may vary depending on the type of counter reactant.[22,23] For example, ZnO ALD commonly employs H_2O, O_2 plasma, and O_3 as the counter reactant, and the growth rate of ALD ZnO films using O_2 plasma is higher than achieved with H_2O and O_3.[22,24–26] This difference is attributed to: (1) differences in the reactivity of the counter reactants with the adsorbed precursor and (2) different surface species that remain after the counter reactant half-reactions. For the latter, H_2O and O_2 plasma leave an OH-terminated surface, while O_3 forms an O-terminated surface in most cases of ALD, resulting in different growth characteristics depending on the reactant.[17,21] From this knowledge, it is logically deduced that adsorption of the precursor could be controlled in each half-cycle by using different counter reactants, which affords control of the surface terminations. Several studies have reported the use of two types of reactants in one ALD cycle. However, there is no detailed study on the effects of terminal surface groups on the film growth characteristics.[27–31] The growth behavior and electrical properties of ALD films formed by using multiple reactants have been reported based

[a]Department of Materials Science and Engineering, Incheon National University, Incheon, 22012, Korea. E-mail: hbrlee@inu.ac.kr
[b]School of Chemical and Biological Engineering, Seoul National University, 08826, Korea
[c]Department of Chemical Engineering, Hongik University, Seoul, 04066, Korea

†Electronic supplementary information (ESI) available. See DOI: 10.1039/d1dt03465k

‡These authors contributed equally to this work.

on *in situ* analysis. However, the mechanism of the surface reaction using two reactants is not clear.[27]

Herein, we study the effects of H_2O and O_3 as counter reactants on the change in the terminal surface groups and the growth characteristics of ALD HfO_2 thin films. ALD HfO_2 thin films have been actively studied as dielectric layers for metal–oxide–semiconductor field-effect transistors (MOSFETs) and as ferroelectric layers for nonvolatile memory devices.[32–34] The growth characteristics of HfO_2 are comparatively analyzed herein by alternating between H_2O, O_3, and their combinations, as counter reactants, during the reactant half-reaction. Interestingly, when the substrate is sequentially exposed to both H_2O and O_3 as counter reactants in one ALD cycle after the precursor half-reaction, the ALD growth characteristics of the films differ from those of the ALD films formed by using a single reactant. Exposure to each counter-reactant changes the surface termination and oxidizes the precursors in a different manner. When the counter reactants are changed during ALD of the HfO_2 films, the film properties (such as the crystallinity and electrical properties) change significantly. The half-cycle reaction during ALD of HfO_2 films using different counter reactants is studied to understand the mechanisms underlying the changes in the growth characteristics and film properties based on theoretical calculations and density functional theory (DFT) simulations, along with several experimental analyses, including X-ray photoelectron spectroscopy (XPS), transmission electron microscopy (TEM), X-ray diffraction (XRD), and X-ray reflectivity (XRR).

2. Experimental

2.1 HfO_2 ALD

A p-type Si(100) wafer was used as the substrate. The Si substrate was cleaned by sequential ultrasonication in acetone, isopropyl alcohol (IPA) (Samchun Chemicals), deionized water, and subsequent immersion in a buffered oxide enchant solution (BOE) comprises a 6 : 1 volume ratio of 40% NH_4F in water to 49% HF in water for 30 s to remove native oxides. All ALD experiments were performed in a laboratory-built ALD chamber with a quartz-glass tube furnace. For HfO_2 ALD, the substrate temperature was set to the range of 200–310 °C. Tetrakis(dimethylamino)-hafnium (TDMAH; Ocean Bridge Co., Ltd, Korea) was used as the Hf precursor, and H_2O or O_3 was used as the counter reactant. The Hf precursor was contained in a stainless canister heated at 40 °C and H_2O was kept in a glass canister at room temperature. The precursor feeding lines were heated to 10 °C higher than the canister to prevent condensation of the precursor. O_3 was generated by an O_3 generator (WHOZ-10A, Won High Tech) using high-purity O_2 (99.999%) gas, and the O_3 concentration was maintained at 120 g m^{-3}. N_2 was used as both the precursor carrier gas and purge gas, and the flow rates of N_2 gas were 30 sccm and 100 sccm for the carrier and purge, respectively, controlled by a mass flow controller (MFC).

Two types of ALD processes were employed: four-step ALD with a single counter reactant and six-step ALD for film deposition using the two-counter-reactant system. Single-reactant ALD was composed of a TDMAH pulse (4 s), N_2 purge (60 s), H_2O pulse (2 s), and N_2 purge (90 s). For ALD using O_3, the process sequence and conditions were the same, except that H_2O was replaced with O_3. The double reactant ALD was composed of a TDMAH pulse (4 s), N purge (60 s), H_2O pulse (2 s), N_2 purge (90 s), O_3 pulse (2 s), N_2 purge (90 s) or TDMAH pulse (4 s), N_2 purge (60 s), O_3 pulse (2 s), N_2 purge (90 s), H_2O pulse (2 s), and N_2 purge (90 s).

2.2 DFT calculation

To model the HfO_2 surfaces, DFT calculations were carried out under periodic conditions using the Vienna *ab initio* simulation package (VASP).[35,36] The energy was calculated by DFT analysis using the Perdew–Burke–Ernzerhof (PBE) generalized gradient approximation (GGA). Three-layer thick HfO_2 slabs were used to model the surfaces. The plane-wave cutoff energy was set to 450 eV. The *k*-point sampling was generated using the Monkhorst–Pack method, and a grid size of 4 × 4 × 1 was used for structure optimization.[37,38] To calculate the transition state energy, the climbing-image nudged elastic band (CI-NEB) method was used with the same cutoff energy and *k*-point.[39] The following equation expresses the adsorption energies:

$$E = E_{\text{sysytem}} - (E_{\text{substrate}} + E_{\text{adsorbate}})$$

where E is the difference between the energy of the slab after adsorption and the total energy of the clean HfO_2 slab plus the adsorbate, which is negative for exothermic adsorption.[40]

2.3 Analysis

The chemical composition of the films was analyzed by X-ray photoelectron spectroscopy (XPS; PHI 5000 II Versa Probe II, ULVAC) using a monochromatic Al-Kα X-ray source. The crystallinity of the films was analyzed by grazing-incidence angle X-ray diffraction (GI-XRD; SmartLab, Rigaku) using a Cu-Kα source with an incidence angle of 1° and by transmission electron microscopy (TEM; JEM-2100F, JEOL Ltd). Lamella for TEM were fabricated by focused ion beam using Helios G4 (Thermo Fisher Scientific). The film density was measured using X-ray reflectivity (XRR). The thickness of the film was measured by ellipsometry analysis (Elli-SE, Ellipso Technology) in the region of 245–1000 nm (*i.e.*, from −1.24 to 5.06 eV) at an incident angle of 64.885°. A metal–oxide–semiconductor (MOS) structure device was fabricated to investigate the electrical properties based on the capacitance–voltage (*C*–*V*) and current–voltage (*I*–*V*) characteristics of the HfO_2 ALD thin films. To fabricate the MOS structure, an 18 nm HfO_2 film was deposited by ALD, followed by deposition of an Au top electrode using a thermal evaporator. The diameter of the Au top electrode was 160 μm. An In–Ga eutectic alloy was used to form a bottom contact with the Si substrate. The *C*–*V* and leakage *I*–*V* characteristics were investigated using an Agilent

E4980A precision LCR meter and a 4156A precision semiconductor parameter analyzer.

3. Results and discussion

Fig. 1a shows the growth characteristics of the ALD HfO_2 films formed on the Si substrate by using single or double reactants at 200–310 °C. Although the growth per cycle (GPC) curves of the films formed with the four counter reactants showed different trends, almost constant GPCs were observed for all films in the range of 200–275 °C, corresponding to the ALD window of HfO_2, consistent with previous results.[41–43] Above 300 °C, the GPC increased in all cases because the temperature was higher than the decomposition temperature of the TDMAH precursor.[44,45] The saturated GPC of the ALD HfO_2 films deposited using H_2O and O_3 was approximately 0.99 Å per cycle and 1.23 Å per cycle, respectively. Interestingly, when the counter reactant sequence was changed to H_2O–O_3 and O_3–H_2O, the GPC changed to 1.09 Å per cycle and 1.16 Å per cycle, respectively. The additional pulse of O_3 followed by the H_2O pulse leads to an increase in the GPC compared with the H_2O-only pulse, whereas adding H_2O after the O_3 pulse decreases the GPC compared with the O_3-only pulse, as shown in Fig. 1a. For all reactant pulse sequences, the thickness of the HfO_2 film changed consistently as a function of the number of ALD cycles at 275 °C (Fig. 1b) compared to that in Fig. 1a. In addition, almost no nucleation delay was observed on the H-terminated Si surface, consistent with the previous report that showed a negligible nucleation delay in approximately four initial cycles.[46]

The differences in the growth characteristics of the HfO_2 ALD films deposited with single or double reactants can be explained by several aspects, including (1) differences in the reactivity of the reactants for oxidation, (2) changes in the surface termination due to the reactant, and (3) differences in the reactivity of TDMAH on both types of functionalized surfaces. For the first reason, it is well known that O_3 is a stronger oxidant than H_2O. It is difficult for H_2O to remove carbonaceous ligands while these ligands are easily removed by O_3.[20,47] Therefore, in contrast with H_2O, O_3 actively eliminates the ligands of the TDMAH precursor to form HfO_2.[20,48]

On the other hand, the surface terminations formed after exposure to H_2O and O_3 would affect the following reactions. In the typical ALD of HfO_2 films using H_2O as a reactant, H and OH surface species are formed by dissociation of H_2O.[49] The Hf–N bonds of the TDMAH precursor are converted to Hf–O bonds on the surface.[20,27,41] For ALD of the HfO_2 films with O_3, however, the molecular O_3 breaks the Hf–N bonds of the Hf precursor, forming Hf–O bonds. Therefore, the surface is entirely O-terminated and almost no OH-terminations are present on the films after exposure to O_3.[20,41,50]

The dominant surface species after oxidation using H_2O or O_3 as single reactants were OH and O, respectively. Furthermore, the terminations could be modulated by alternate exposure of the substrate to the reactants in the present double reactant approach. DFT calculations in Fig. 2a show that exposure to H_2O changes the O-termination to OH-termination by dissociative adsorption of H_2O; this change can take place in the O_3–H_2O double reactant process. In contrast, subsequent exposure to O_3 after the H_2O pulse can eliminate the OH species on the surface, producing H_2O and O_2 as gaseous byproducts, as shown in Fig. 2b. As a result, the OH-terminated surface can be changed to an O-terminated surface. Therefore, in the double reactant process using H_2O–O_3, the Hf–OH surface formed by the reaction with H_2O is transformed to Hf–O by subsequent exposure to O_3. Similarly, after O_3 exposure, the Hf–O surface is changed to Hf–OH by subsequent exposure to H_2O in the case of the O_3–H_2O double reactant.

The GPC in the H_2O–O_3 double reactant process was higher than that in the H_2O single reactant process, whereas the GPC in the O_3–H_2O double reactant process was lower than that in the O_3 single reactant process. Therefore, the GPC in the double-reactant ALD differs from that in the respective single processes because of the higher reactivity of TDMAH on the O-terminated surface than on the OH-terminated surface. The protons on the O-terminated surface are available for the dis-

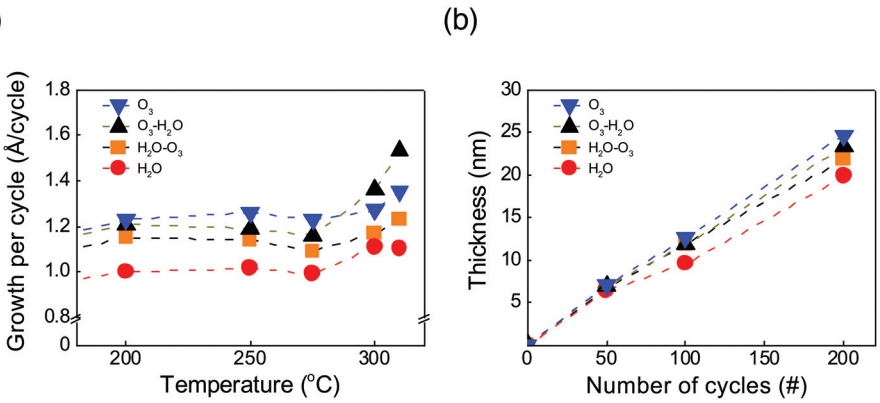

Fig. 1 (a) Growth characteristics of ALD HfO_2 films formed at various temperatures using different reactants, (b) thickness *versus* ALD cycle number using each reactant.

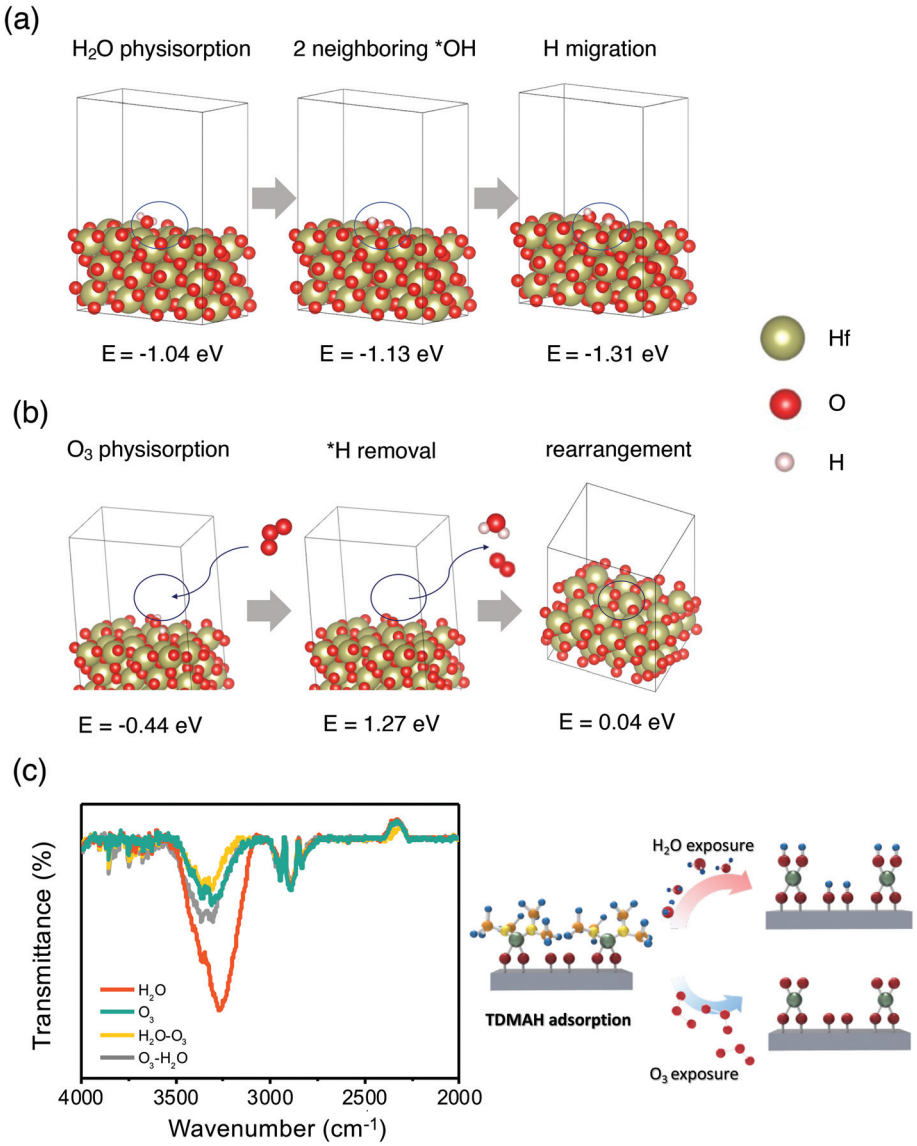

Fig. 2 DFT calculation on surface termination for each reactant species: (a) O_3–H_2O process, (b) H_2O–O_3 process. (c) FT-IR spectra of HfO_2 using each reactant and schematic of change in surface termination in HfO_2 film upon exposure to each reactant.

sociation of ligand fragments.[30] These protons frequently travel between oxygen and nitrogen and may be considered to be shared between oxygen and nitrogen. In other words, multiple ligands become protonated before the desorption commences. On the O-terminated surface, Hf is surrounded by more oxygens. In this case, the proton may travel a shorter distance to attach to the nitrogen than on the OH-terminated surface. Therefore, proton diffusion from the O-terminated surface to the N of TDMAH has a relatively low barrier and is an exothermic process.[30] Therefore, it is expected that the surface O will be more reactive toward TDMAH adsorption during subsequent exposure to the precursor. In addition, desorption of H_2O when the O-terminated surface is exposed to H_2O depletes the surface of reactive protons for the dissociation of TDMAH ligand fragments.[30] Thus, the lower GPC of HfO_2 using the O_3–H_2O reactant is attributed to the change in the surface termination. For the four reactant systems, simulation of the reaction with different reaction rate constants showed a similar trend (see Fig. S1 in the ESI†).

Fig. 2c shows the FT-IR spectrum of each HfO_2 film. For all samples, peaks were observed at 3200–3550 cm^{-1}, corresponding to OH absorption. Comparing the H_2O and O_3 processes, the spectrum of the HfO_2 film formed by ALD with H_2O shows a stronger OH absorption peak than that formed using the O_3 process. This means that for the H_2O process, there is a higher OH concentration in the film or on the surface due to the formation of an OH-terminated surface during the reaction. The OH peak of HfO_2 formed with O_3 was also less intense than that of the film formed with H_2O. The OH peak of the HfO_2 film formed with O_3 was assumed to be

due to byproducts such as CO_2, H_2O, and CH_2O, which are formed when the TDMAH precursor reacts with the O_3 reactant.[41] The H_2O byproduct can partially form an Hf–OH terminated surface instead of an Hf–O-terminated surface during the reactant half-reaction.[41] For the film formed by using the double reactants, the OH peak was significantly less intense compared to that for the film formed with H_2O. The FT-IR data may provide indirect evidence that O_3 pulse after H_2O pulse changes the OH-terminated surface to the O-terminated surface, consistent with the DFT calculation. Comparing the data for the films formed by the O_3 and O_3–H_2O processes, the intensity of the OH absorption peak also increased after the H_2O pulse. This means that the H_2O pulse after O_3 pulse can partially change the O-terminated surface to an OH-terminated surface, as explained above. The schematic illustration in Fig. 2c shows how the surface termination varies depending on the reactant in the HfO_2 ALD reaction. The precursor adsorption reaction is closely related to the terminal surface groups.[51–53]

Fig. 3 shows the Hf 4f XPS profiles of the HfO_2 films formed by ALD at 275 °C, using H_2O, O_3, H_2O–O_3, and O_3–H_2O reactants. All four spectra show two main peaks at 18.2 and 16.5 eV, corresponding to Hf $4f_{5/2}$ and $4f_{7/2}$, respectively. In addition to the Hf $4f_{5/2}$ and $4f_{7/2}$ peaks, two other peaks were found at lower energy. Due to the existence of defects such as oxygen vacancies (V_{ox}), oxygen interstitials (O_i), and Hf intersti-

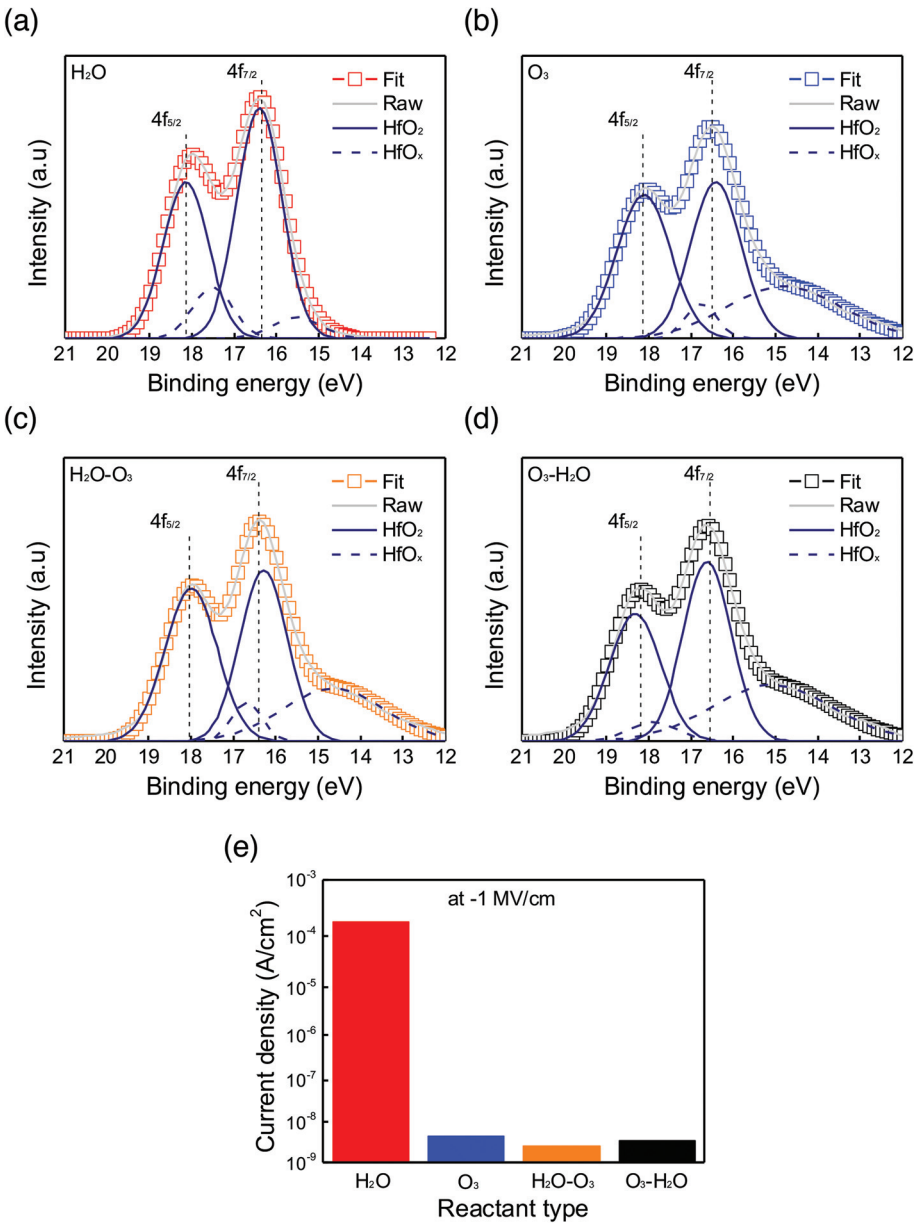

Fig. 3 XPS profiles of HfO_2 films formed using each reactant process: (a) H_2O, (b) O_3, (c) H_2O–O_3, (d) O_3–H_2O, and (e) leakage current density from *I*–*V* curve using 18 nm ALD HfO_2 film deposited at 275 °C.

Table 1 Chemical composition of HfO_2 films deposited at 275 °C

	Hf (%)		O (%)		Impurity (%)	
Reactant type	HfO_2	HfO_x	O–Hf	O–H	C	N
H_2O	24.81	4.45	53.75	5.71	7.23	4.05
H_2O–O_3	25.97	10.66	60.95	2.41	<1	<1
O_3	25.88	11.78	59.65	2.68	<1	<1
O_3–H_2O	25.26	13.01	57.22	4.50	<1	<1

tials, Hf sub-oxides (HfO_x, $x < 2$) were formed,[54–56] the signals of which are typically found in a lower energy range than that of HfO_2.[56–59] The atomic percentages of the bonds in the HfO_2 films formed with different reactants are listed in Table 1. Theoretically, V_{ox} and O_i can be considered as point defects in the HfO_2 lattice,[55,60] which become larger and more stable under O-rich conditions.[60–63] During the O_3, O_3–H_2O, H_2O–O_3 pulses, which provide O-rich conditions, it is expected that the

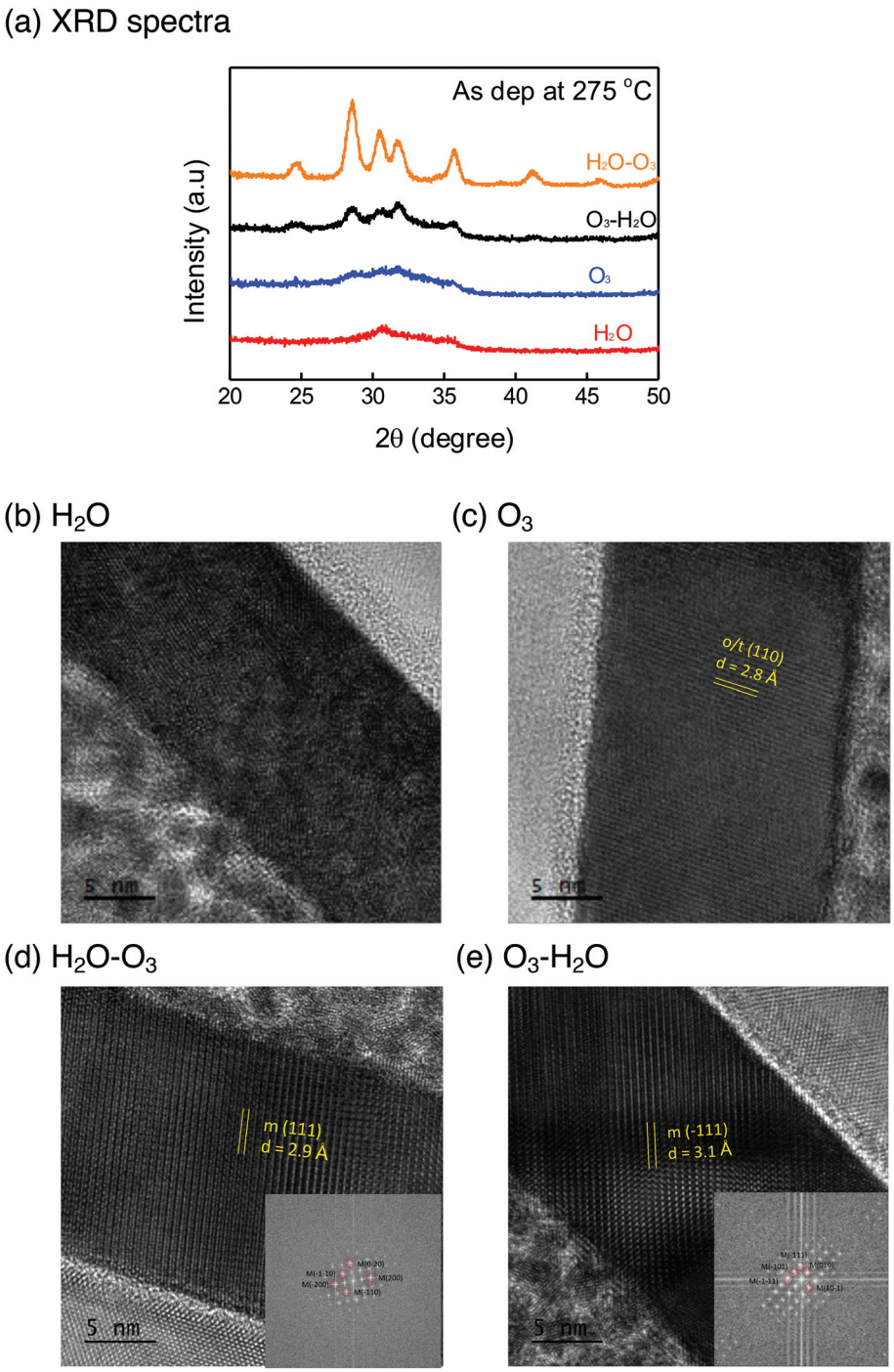

Fig. 4 (a) XRD spectra of as-deposited HfO_2 film formed at 275 °C, and TEM image of HfO_2 film grown at 275 °C using each reactant process: (b) H_2O, (c) O_3, (d) H_2O–O_3, (e) O_3–H_2O.

numbers of these point defects will increase, leading to increased formation of HfO_x sub-oxides. Consistently, the amounts of HfO_x sub-oxides in the double reactant pulses are larger than in the case of a single H_2O pulse (Table 1).

Because O_3 is a stronger oxidant that the other species, the reactants containing O_3, such as O_3, O_3–H_2O, and H_2O–O_3, react with the ligand completely.[20,56] However, a single H_2O pulse is likely to result in incomplete reaction with remaining oxygen radicals such as C–O or C–OH.[20,56,58] Thus, more impurities (7.23% C and 4.05% N) were detected in the ALD HfO_2 film formed by deposition with H_2O due to incomplete reaction. Fig. 3e shows the leakage current densities measured at an electric field of −1 MV cm^{-1} using the Au/HfO_2/Si MOS structure. The results show a low leakage current of 4.55×10^{-9}, 3.6×10^{-9}, and 2.6×10^{-9} A cm^{-2} for O_3, O_3–H_2O, and H_2O–O_3, respectively, which are comparable with the previous results for HfO_2, whereas for the HfO_2 film formed by using H_2O, the leakage current was much higher (1.87×10^{-4} A cm^{-2}). The high leakage current of the film formed with H_2O as a reactant can be attributed to the high level of C and N impurities in the HfO_2 film.[64,65]

Fig. 4a presents the XRD data for the ALD HfO_2 film formed at 275 °C. Typically, HfO_2 films formed by using the TDMAH precursor remain amorphous in the absence of post-deposition annealing.[32,66] Interestingly, however, the XRD profiles of the HfO_2 films formed by using the double reactant (O_3–H_2O and H_2O–O_3) show strong peaks of crystalline species despite the lack of a high-temperature annealing process (Fig. 4a). The peaks observed at 28.5°, 31.6°, 35.5°, and 40.9° are due to the ($\bar{1}11$), (111), (200), and ($\bar{2}11$) planes of monoclinic phases, respectively. In addition, a peak corresponding to a mixture of orthorhombic and tetragonal phases (111) was also observed at 30.4°.[67,68] In contrast with the pattern of the film formed by using the double reactant, there was almost no strong peak in the XRD spectrum of the HfO_2 films formed by using H_2O and O_3 single reactants, except for a very small peak at 30.4° in the pattern of the HfO_2 film formed by using H_2O.

To better understand this crystallization phenomenon, TEM images of the HfO_2 films deposited at 275 °C, with a thickness of 17 nm, were obtained as shown in Fig. 4b–e. The HfO_2 film formed by the H_2O single pulse comprised an amorphous phase with small crystallites (Fig. 4b). It has been reported that the remaining C–O bonds from the insufficient oxidation reaction become a key factor in the formation of the tetragonal phase.[50,69] Thus, a very weak peak indexed to the tetragonal phase was observed at 30.4° in the XRD pattern. As shown in Fig. 4c, vague crystalline fringes were observed, but the overall crystallinity of HfO_2 formed by ALD with O_3 was not very defined. Owing to this low crystallinity, there was no strong XRD peak in Fig. 4a.

Fig. 4d and e show that the films formed using the double reactants (H_2O–O_3 and O_3–H_2O) were fully crystallized. When an additional O_3 pulse was performed after the H_2O pulse, the profile of the HfO_2 film showed clear crystalline fringes (Fig. 4d) with a *d*-spacing of 2.9 Å, corresponding to the monoclinic (111) plane. Similarly, the HfO_2 film prepared using O_3–H_2O shows a clear crystalline structure with a measured *d*-spacing of 3.1 Å (Fig. 4e), consistent with the ($\bar{1}11$) plane of the monoclinic structure.[67,70] These results show that the HfO_2 films prepared using the double reactants have polycrystalline microstructures even without annealing, which is consistent with the XRD results in Fig. 4a. As discussed, the densities of V_{ox} and O_i point defects increase under O-rich conditions,[60–63] affecting the formation of the monoclinic HfO_2 phase.[61,71] Thus, the double reactant process provides O-rich conditions, leading to an increase in the defect density in the lattice. The defects (V_{ox} and O_i) in the lattice are known nucleation sites for the crystallization of oxide films.[72,73] In addition, it was reported that O_i defects may initiate the nucleation of monoclinic HfO_2.[61] As the number of ALD cycles increased, the defects formed with the double reactant contributed to the formation of crystallite nuclei, leading to crystal growth,[64] as observed in the XRD and TEM results.

4. Conclusion

The effect of H_2O, O_3, and their combinations on the growth behavior and film properties of ALD HfO_2 were investigated. The GPC for the HfO_2 film formed by ALD using a single O_3 reactant is higher than that of the film formed by using H_2O because O_3 is a stronger oxidant, which leads to formation of an O-terminated surface that is more reactive for TDMAH adsorption. The terminal groups formed after exposure to the first reactant (half-cycle) changed during subsequent exposure to the other reactant, such as in the O_3–H_2O or H_2O–O_3 cycles, resulting in different growth rates. The single and double reactants affect the formation of defect sites, V_{ox} and O_i, in the HfO_2 films due to the different oxidation conditions. Highly crystallized HfO_2 films were formed with the use of the double-reactant, without additional annealing, but not in the case of the single-reactant. The defects are known nuclei for crystallization, and thus promote the formation of a polycrystalline microstructure during ALD of HfO_2. From this study, control of the surface terminal groups by changing the reactant combination significantly improves the properties of ALD films, and this approach can be easily applied to other material systems. For example, based on our previous results that showed Ru ALD by using both of H_2O and O_2 counter reactants,[74] the termination of Ru can be controlled by H_2O and O_2 to modify the film properties and growth characteristics.

Conflicts of interest

There are no conflicts to declare.

Acknowledgements

This work was supported by the Incheon National University Research Grant in 2018-0467 and by the MOTIE (Ministry of

Trade, Industry & Energy; project no. 20011970) and the Korea Semiconductor Research Consortium (KSRC) support program for the development of future semiconductor devices.

References

1 S. M. George, Atomic layer deposition: An overview, *Chem. Rev.*, 2010, **110**, 111–131, DOI: 10.1021/cr900056b.
2 J. T. Gaskins, P. E. Hopkins, D. R. Merrill, S. R. Bauers, E. Hadland, D. C. Johnson, *et al.*, Review—Investigation and Review of the Thermal, Mechanical, Electrical, Optical, and Structural Properties of Atomic Layer Deposited High-k Dielectrics: Beryllium Oxide, Aluminum Oxide, Hafnium Oxide, and Aluminum Nitride, *ECS J. Solid State Sci. Technol.*, 2017, **6**, N189–N208, DOI: 10.1149/2.0091710jss.
3 M. Leskelä and M. Ritala, Atomic layer deposition (ALD): from precursors to thin film structures, *Thin Solid Films*, 2002, **409**, 138–146, DOI: 10.1016/S0040-6090(02)00117-7.
4 R. W. Johnson, A. Hultqvist and S. F. Bent, A brief review of atomic layer deposition: From fundamentals to applications, *Mater. Today*, 2014, **17**, 236–246, DOI: 10.1016/j.mattod.2014.04.026.
5 Y. Wu, D. Döhler, M. Barr, E. Oks, M. Wolf, L. Santinacci, *et al.*, Atomic Layer Deposition from Dissolved Precursors, *Nano Lett.*, 2015, **15**, 6379–6385, DOI: 10.1021/acs.nanolett.5b01424.
6 R. Chen, Y.-C. Li, J.-M. Cai, K. Cao and H.-B.-R. Lee, Atomic level deposition to extend Moore's law and beyond, *Int. J. Extreme Manuf.*, 2020, **2**, 022002, DOI: 10.1088/2631-7990/ab83e0.
7 H. C. M. Knoops, S. E. Potts, A. A. Bol and W. M. M. Kessels, *Atomic Layer Deposition. Handbook of Crystal Growth*, Elsevier, 2015, pp. 1101–1134. DOI: 10.1016/B978-0-444-63304-0.00027-5.
8 M. D. Groner, J. W. Elam, F. H. Fabreguette and S. M. George, Electrical characterization of thin Al2O3 films grown by atomic layer deposition on silicon and various metal substrates, *Thin Solid Films*, 2002, **413**, 186–197, DOI: 10.1016/S0040-6090(02)00438-8.
9 S. D. Elliott, Atomic-scale simulation of ALD chemistry, *Semicond. Sci. Technol.*, 2012, **27**(7), 074008, DOI: 10.1088/0268-1242/27/7/074008.
10 R. L. Puurunen, W. Vandervorst, W. F. A. Besling, O. Richard, H. Bender, T. Conard, *et al.*, Island growth in the atomic layer deposition of zirconium oxide and aluminum oxide on hydrogen-terminated silicon: Growth mode modeling and transmission electron microscopy, *J. Appl. Phys.*, 2004, **96**, 4878–4889, DOI: 10.1063/1.1787624.
11 R. Chen and S. F. Bent, Chemistry for Positive Pattern Transfer Using Area-Selective Atomic Layer Deposition, *Adv. Mater.*, 2006, **18**, 1086–1090, DOI: 10.1002/adma.200502470.
12 A. J. M. Mackus, M. J. M. Merkx and W. M. M. Kessels, From the Bottom-Up: Toward Area-Selective Atomic Layer Deposition with High Selectivity, *Chem. Mater.*, 2019, **31**, 2–12, DOI: 10.1021/acs.chemmater.8b03454.
13 D. V. Nazarov, M. Y. Maximov, P. A. Novikov, A. A. Popovich, A. O. Silin, V. M. Smirnov, *et al.*, Atomic layer deposition of tin oxide using tetraethyltin to produce high-capacity Li-ion batteries, *J. Vac. Sci. Technol., A*, 2017, **35**, 01B137, DOI: 10.1116/1.4972554.
14 V. Miikkulainen, M. Leskelä, M. Ritala and R. L. Puurunen, Crystallinity of inorganic films grown by atomic layer deposition: Overview and general trends, *J. Appl. Phys.*, 2013, **113**(2), 021301, DOI: 10.1063/1.4757907.
15 L. Baker, A. S. Cavanagh, D. Seghete, S. M. George, A. J. M. MacKus, W. M. M. Kessels, *et al.*, Nucleation and growth of Pt atomic layer deposition on Al_2O_3 substrates using (methylcyclopentadienyl)-trimethyl platinum and O_2 plasma, *J. Appl. Phys.*, 2011, **109**(8), 084333, DOI: 10.1063/1.3555091.
16 H. B. Profijt, S. E. Potts, M. C. M. van de Sanden and W. M. M. Kessels, Plasma-Assisted Atomic Layer Deposition: Basics, Opportunities, and Challenges, *J. Vac. Sci. Technol., A*, 2011, **29**, 050801, DOI: 10.1116/1.3609974.
17 H. G. Kim and H. B. R. Lee, Atomic Layer Deposition on 2D Materials, *Chem. Mater.*, 2017, **29**, 3809–3826, DOI: 10.1021/acs.chemmater.6b05103.
18 Y. Cho, S. H. Kim, B. S. Kim, Y. Kim and W. Jeon, Modulation of the adsorption chemistry of a precursor in atomic layer deposition to enhance the growth per cycle of a TiO2 thin film, *Phys. Chem. Chem. Phys.*, 2021, **23**, 2568–2574, DOI: 10.1039/D0CP04176A.
19 S. Seo, W. J. Woo, Y. Lee, H. Yoon, M. Kim, I.-K. Oh, *et al.*, Reaction Mechanisms of Non-hydrolytic Atomic Layer Deposition of Al2O3 with a Series of Alcohol Oxidants, *J. Phys. Chem. C*, 2021, **125**, 18151–18160, DOI: 10.1021/acs.jpcc.1c03518.
20 S. Y. Lee, H. K. Kim, J. H. Lee, I. H. Yu, J. H. Lee and C. S. Hwang, Effects of O3 and H_2O as oxygen sources on the atomic layer deposition of HfO2 gate dielectrics at different deposition temperatures, *J. Mater. Chem. C*, 2014, **2**, 2558–2568, DOI: 10.1039/c3tc32561j.
21 S. C. Ha, E. Choi, S. H. Kim and J. S. Roh, Influence of oxidant source on the property of atomic layer deposited Al 2 O 3 on hydrogen-terminated Si substrate, *Thin Solid Films*, 2005, **476**, 252–257, DOI: 10.1016/j.tsf.2004.09.035.
22 S. K. Kim, C. S. Hwang, S. H. K. Park and S. J. Yun, Comparison between ZnO films grown by atomic layer deposition using H 2O or O3 as oxidant, *Thin Solid Films*, 2005, **478**, 103–108, DOI: 10.1016/j.tsf.2004.10.015.
23 M. Cho, H. B. Park, J. Park, S. W. Lee, C. S. Hwang, J. Jeong, *et al.*, Comparison of properties of an Al 2 O 3 thin layers grown with remote O 2 plasma, H 2 O, or O 3 as oxidants in an ALD process for HfO 2 gate dielectrics, *J. Electrochem. Soc.*, 2005, **152**, 1–5, DOI: 10.1149/1.1884130.
24 Z. Baji, Z. Lábadi, Z. E. Horváth, G. Molnár, J. Volk, I. Bársony, *et al.*, Nucleation and growth modes of ALD

ZnO, *Cryst. Growth Des.*, 2012, **12**, 5615–5620, DOI: 10.1021/cg301129v.

25 E. Guziewicz, M. Godlewski, L. Wachnicki, T. A. Krajewski, G. Luka, S. Gieraltowska, *et al.*, ALD grown zinc oxide with controllable electrical properties, *Semicond. Sci. Technol.*, 2012, **27**(7), 074011, DOI: 10.1088/0268-1242/27/7/074011.

26 D. Kim, H. Kang, J. M. Kim and H. Kim, The properties of plasma-enhanced atomic layer deposition (ALD) ZnO thin films and comparison with thermal ALD, *Appl. Surf. Sci.*, 2011, **257**, 3776–3779, DOI: 10.1016/j.apsusc.2010.11.138.

27 J. A. Libera, J. N. Hryn and J. W. Elam, Indium oxide atomic layer deposition facilitated by the synergy between oxygen and water, *Chem. Mater.*, 2011, **23**, 2150–2158, DOI: 10.1021/cm103637t.

28 T. Kubo, J. J. Freedsman, Y. Iwata and T. Egawa, Electrical properties of GaN-based metal-insulator-semiconductor structures with Al_2O_3 deposited by atomic layer deposition using water and ozone as the oxygen precursors, *Semicond. Sci. Technol.*, 2014, **29**(4), 045004, DOI: 10.1088/0268-1242/29/4/045004.

29 X. Cheng, P. Repo, H. Halvard, A. P. Perros, E. S. Marstein, M. Di Sabatino, *et al.*, Surface Passivation Properties of HfO2 Thin Film on n-Type Crystalline Si, *IEEE J. Photovolt.*, 2017, **7**, 479–485, DOI: 10.1109/JPHOTOV.2016.2645399.

30 M. Shirazi and S. D. Elliott, Multiple proton diffusion and film densification in atomic layer deposition modeled by density functional theory, *Chem. Mater.*, 2013, **25**, 878–889, DOI: 10.1021/cm303630e.

31 M. Li, D. Gao, S. Li, Z. Zhou, J. Zou, H. Tao, *et al.*, Realization of highly-dense Al2O3 gas barrier for top-emitting organic light-emitting diodes by atomic layer deposition, *RSC Adv.*, 2015, **5**, 104613–104620, DOI: 10.1039/c5ra21424f.

32 J. H. Choi, Y. Mao and J. P. Chang, Development of hafnium based high-k materials - A review, *Mater. Sci. Eng., R*, 2011, **72**, 97–136, DOI: 10.1016/j.mser.2010.12.001.

33 M. H. Park, Y. H. Lee, H. J. Kim, Y. J. Kim, T. Moon, K. K. Do, *et al.*, Ferroelectricity and Antiferroelectricity of Doped Thin HfO2-Based Films, *Adv. Mater.*, 2015, **27**, 1811–1831, DOI: 10.1002/adma.201404531.

34 D. Bräuhaus, S. Mueller, U. Schröder, U. Böttger, L. Frey, T. S. Böscke, *et al.*, Ferroelectricity in Simple Binary ZrO 2 and HfO 2, *Nano Lett.*, 2012, **12**, 4318–4323, DOI: 10.1021/nl302049k.

35 G. Kresse and J. Hafner, Ab initio molecular dynamics for liquid metals, *Phys. Rev. B: Condens. Matter Mater. Phys.*, 1993, **47**, 558–561, DOI: 10.1103/PhysRevB.47.558.

36 G. Kresse and J. Furthmüller, Efficiency of *ab initio* total energy calculations for metals and semiconductors using a plane-wave basis set, *Comput. Mater. Sci.*, 1996, **6**, 15–50, DOI: 10.1016/0927-0256(96)00008-0.

37 A. B. Mukhopadhyay, J. F. Sanz and C. B. Musgrave, First-principles investigation of hydroxylated monoclinic HfO 2 surfaces, *Chem. Mater.*, 2006, **18**, 3397–3403, DOI: 10.1021/cm060679r.

38 L. Li, X. Huang, Y. F. Zhang, X. Guo and W. K. Chen, First-principles investigation of H 2 O on HfO 2 (1 1 0) surface, *Appl. Surf. Sci.*, 2013, **264**, 424–432, DOI: 10.1016/j.apsusc.2012.10.038.

39 G. Henkelman, B. P. Uberuaga and H. Jónsson, Climbing image nudged elastic band method for finding saddle points and minimum energy paths, *J. Chem. Phys.*, 2000, **113**, 9901–9904, DOI: 10.1063/1.1329672.

40 Z. Chafi, N. Keghouche and C. Minot, DFT study of Ni-CeO_2 interaction: Adsorption and insertion, *Surf. Sci.*, 2007, **601**, 2323–2329, DOI: 10.1016/j.susc.2007.03.041.

41 X. Liu, S. Ramanathan, A. Longdergan, A. Srivastava, E. Lee, T. E. Seidel, *et al.*, ALD of Hafnium Oxide Thin Films from Tetrakis(ethylmethylamino)hafnium and Ozone, *J. Electrochem. Soc.*, 2005, **152**, G213, DOI: 10.1149/1.1859631.

42 I. K. Oh, J. Tanskanen, H. Jung, K. Kim, M. J. Lee, Z. Lee, *et al.*, Nucleation and Growth of the HfO_2 Dielectric Layer for Graphene-Based Devices, *Chem. Mater.*, 2015, **27**, 5868–5877, DOI: 10.1021/acs.chemmater.5b01226.

43 S. Park, B. E. Park, H. Yoon, S. Lee, T. Nam, T. Cheon, *et al.*, Comparative study on atomic layer deposition of HfO2: Via substitution of ligand structure with cyclopentadiene, *J. Mater. Chem. C*, 2020, **8**, 1344–1352, DOI: 10.1039/c9tc05778a.

44 N. K. Oh, J.-T. Kim, J.-K. Ahn, G. Kang, S. Y. Kim and J.-Y. Yun, The Effects of Thermal Decomposition of Tetrakis-ethylmethylaminohafnium (TEMAHf) Precursors on HfO_2 Film Growth using Atomic Layer Deposition, *Appl. Sci. Converg. Technol.*, 2016, **25**, 56–60, DOI: 10.5757/ASCT.2016.25.3.56.

45 P. D. Kirsch, M. A. Quevedo-Lopez, H.-J. Li, Y. Senzaki, J. J. Peterson, S. C. Song, *et al.*, Nucleation and growth study of atomic layer deposited HfO2 gate dielectrics resulting in improved scaling and electron mobility, *J. Appl. Phys.*, 2006, **99**, 023508, DOI: 10.1063/1.2161819.

46 J. C. Hackley, J. D. Demaree and T. Gougousi, Atomic Layer Deposition of HfO_2 Thin Films on Si and GaAs Substrates, *MRS Proc.*, 2007, **1073**(1), 1–6, DOI: 10.1557/PROC-1073-H04-19.

47 A. S. Ansari, S. S. Raya and B. Shong, Mechanistic Investigation on Thermal Atomic Layer Deposition of Group 13 Oxides, *J. Phys. Chem. C*, 2020, **124**, 17121–17134, DOI: 10.1021/acs.jpcc.0c04872.

48 M. Cho, D. S. Jeong, J. Park, H. B. Park, S. W. Lee and T. J. Park, Comparison between atomic-layer-deposited HfO_2 films using O_3 or H_2O oxidant and $Hf[N(CH_3)_2]_4$ precursor, *Appl. Phys. Lett.*, 2004, **85**(24), 5953–5955, DOI: 10.1063/1.1829773.

49 F. McBride and A. Hodgson, Water and its partially dissociated fragments at metal surfaces, *Int. Rev. Phys. Chem.*, 2017, **36**, 1–38, DOI: 10.1080/0144235X.2016.1253244.

50 D. Y. Cho, H. S. Jung, I. H. Yu, J. H. Yoon, H. K. Kim, S. Y. Lee, *et al.*, Stabilization of tetragonal HfO 2 under low active oxygen source environment in atomic layer depo-

sition, *Chem. Mater.*, 2012, **24**, 3534–3543, DOI: 10.1021/cm3001199.

51 J. Lu, K.-B. Low, Y. Lei, J. A. Libera, A. Nicholls, P. C. Stair, *et al.*, Toward atomically-precise synthesis of supported bimetallic nanoparticles using atomic layer deposition, *Nat. Commun.*, 2014, **5**, 3264, DOI: 10.1038/ncomms4264.

52 A. Mameli, B. Karasulu, M. A. Verheijen, B. Barcones, B. Macco, A. J. M. Mackus, *et al.*, Area-Selective Atomic Layer Deposition of ZnO by Area Activation Using Electron Beam-Induced Deposition, *Chem. Mater.*, 2019, **31**, 1250–1257, DOI: 10.1021/acs.chemmater.8b03165.

53 J. Soethoudt, S. Crahaij, T. Conard and A. Delabie, Impact of SiO2 surface composition on trimethylsilane passivation for area-selective deposition, *J. Mater. Chem. C*, 2019, **7**, 11911–11918, DOI: 10.1039/C9TC04091A.

54 D. R. Islamov, V. N. Kruchinin, V. Aliev, T. V. Perevalov, V. A. Gritsenko, I. P. Prosvirin, *et al.*, Potential Fluctuation in RRAM Based on Non-Stoichiometric Hafnium Sub-Oxides, *Adv. Sci. Technol.*, 2016, **99**, 69–74, DOI: 10.4028/www.scientific.net/AST.99.69.

55 S. R. Bradley, *Computational Modelling of Oxygen Defects and Interfaces in Monoclinic HfO2*, UCL, University College, London, 2016, pp. 146.

56 A. S. Sokolov, Y.-R. Jeon, S. Kim, B. Ku, D. Lim, H. Han, *et al.*, Influence of oxygen vacancies in ALD HfO2-x thin films on non-volatile resistive switching phenomena with a Ti/HfO2-x/Pt structure, *Appl. Surf. Sci.*, 2018, **434**, 822–830, DOI: 10.1016/j.apsusc.2017.11.016.

57 N. YuN and V. A. Gritsenko, Short-range order in amorphous SiO_x by x ray photoelectron spectroscopy, *J. Appl. Phys.*, 2011, **110**, 014107, DOI: 10.1063/1.3606422.

58 I. K. Oh, B. E. Park, S. Seo, B. C. Yeo, J. Tanskanen, H. B. R. Lee, *et al.*, Comparative study of the growth characteristics and electrical properties of atomic-layer-deposited HfO2 films obtained from metal halide and amide precursors, *J. Mater. Chem. C*, 2018, **6**, 7367–7376, DOI: 10.1039/c8tc01476k.

59 R. Zazpe, M. Ungureanu, F. Golmar, P. Stoliar, R. Llopis, F. Casanova, *et al.*, Resistive switching dependence on atomic layer deposition parameters in HfO2-based memory devices, *J. Mater. Chem. C*, 2014, **2**, 3204–3211, DOI: 10.1039/c3tc31819b.

60 C. Künneth, R. Batra, G. A. Rossetti, R. Ramprasad and A. Kersch, Chapter 6 - Thermodynamics of Phase Stability and Ferroelectricity From First Principles, in *Ferroelectricity in Doped Hafnium Oxide: Materials, Properties and Devices*, ed. U. Schroeder, C. S. Hwang and H. Funakubo, Woodhead Publishing, 2019, pp. 245–289. DOI: 10.1016/B978-0-08-102430-0.00006-1.

61 J. L. Lyons, A. Janotti and C. G. Van de Walle, The role of oxygen-related defects and hydrogen impurities in HfO2 and ZrO2, *Microelectron. Eng.*, 2011, **88**, 1452–1456, DOI: 10.1016/j.mee.2011.03.099.

62 E. Hildebrandt, J. Kurian, M. M. Müller, T. Schroeder, H.-J. Kleebe and L. Alff, Controlled oxygen vacancy induced p -type conductivity in HfO_{2-x}, thin films, *Appl. Phys. Lett.*, 2011, **99**, 112902, DOI: 10.1063/1.3637603.

63 S. Clima, Y. Y. Chen, C. Y. Chen, L. Goux, B. Govoreanu, R. Degraeve, *et al.*, First-principles thermodynamics and defect kinetics guidelines for engineering a tailored RRAM device, *J. Appl. Phys.*, 2016, **119**, 225107, DOI: 10.1063/1.4953673.

64 D. M. Hausmann and R. G. Gordon, Surface morphology and crystallinity control in the atomic layer deposition (ALD) of hafnium and zirconium oxide thin films, *J. Cryst. Growth*, 2003, **249**, 251–261, DOI: 10.1016/S0022-0248(02)02133-4.

65 A. Monshi, M. R. Foroughi and M. R. Monshi, Modified Scherrer Equation to Estimate More Accurately Nano-Crystallite Size Using XRD, *World J. Nano Sci. Eng.*, 2012, **02**, 154–160, DOI: 10.4236/wjnse.2012.23020.

66 J. Niinistö, K. Kukli, M. Heikkilä, M. Ritala and M. Leskelä, Atomic layer deposition of high-k oxides of the Group 4 metals for memory applications, *Adv. Eng. Mater.*, 2009, **11**, 223–234, DOI: 10.1002/adem.200800316.

67 C. Palade, A.-M. Lepadatu, A. Slav, O. Cojocaru, A. Iuga, V. A. Maraloiu, *et al.*, A nanoscale continuous transition from the monoclinic to ferroelectric orthorhombic phase inside HfO_2 nanocrystals stabilized by HfO_2 capping and self-controlled Ge doping, *J. Mater. Chem. C*, 2021, **9**(36), 12353–12366, DOI: 10.1039/D1TC02921E.

68 M. Lapteva, V. Beladiya, S. Riese, P. Hanke, F. Otto, T. Fritz, *et al.*, Influence of temperature and plasma parameters on the properties of PEALD HfO_2, *Opt. Mater. Express*, 2021, **11**, 1918, DOI: 10.1364/OME.422156.

69 A. Kashir, H. W. Kim, S. Oh and H. Hwang, Large remnant polarization in a wake-up free Hf0.5Zr0.5O2 ferroelectric film through bulk and interface engineering n.d.:24.

70 X.-Y. Zhang, C.-H. Hsu, S.-Y. Lien, W.-Y. Wu, S.-L. Ou, S.-Y. Chen, *et al.*, Temperature-Dependent HfO2/Si Interface Structural Evolution and its Mechanism, *Nanoscale Res. Lett.*, 2019, **14**, 83, DOI: 10.1186/s11671-019-2915-0.

71 P. McIntyre, Bulk and Interfacial Oxygen Defects in HfO2 Gate Dielectric Stacks: A Critical Assessment, *ECS Trans.*, 2019, **11**, 235–249, DOI: 10.1149/1.2779564.

72 J. Strand, M. Kaviani, D. Gao, A.-M. El-Sayed, V. V. Afanas'ev and A. L. Shluger, Intrinsic charge trapping in amorphous oxide films: status and challenges, *J. Phys.: Condens. Matter*, 2018, **30**, 233001, DOI: 10.1088/1361-648X/aac005.

73 S. R. Bradley, G. Bersuker and A. L. Shluger, Modelling of oxygen vacancy aggregates in monoclinic HfO2: can they contribute to conductive filament formation?, *J. Phys.: Condens. Matter*, 2015, **27**, 415401, DOI: 10.1088/0953-8984/27/41/415401.

74 C. T. Nguyen, J. Yoon, R. Khan, B. Shong and H.-B.-R. Lee, Thermal atomic layer deposition of metallic Ru using H_2O as a reactant, *Appl. Surf. Sci.*, 2019, **488**, 896–902, DOI: 10.1016/j.apsusc.2019.05.242.

